Inorg. Chem. **2006**, *45*, 5328–5337

Synthesis, Structural Characterization, Experimental, and Computational Spectrophotometric Studies of 8-Quinolinyloxymethyphosphonate Compounds

Siud Pui Man,[†] David M. Benoit,*[,‡] Ester Buchaca,[†] Fola Esan,[†] Majid Motevalli,[†] John Wilson,[†] and Alice Sullivan*[,†]

School of Biological and Chemical Sciences, Queen Mary, University of London, Mile End Road, E1 4NS, U.K., and Nachwuchsgruppe Theorie - SFB 569, Albert-Einstein-Allee 11, University of Ulm, D-89081 Ulm, Germany

Received December 5, 2005

The synthesis of diethyl-8-quinolinyloxymethylphosphonate **1** and 8-quinolinyloxymethylphosphonic acid hemihydroiodide **2** is reported along with their spectroscopic and analytical characteristics (NMR, infrared, mass spectra, and elemental analysis). The single-crystal X-ray structure of **2** is described. Solutions of the disodium phosphonate **3**, from **2** and sodium hydroxide, were prepared and used in situ. The coordination complex between **1** and zinc chloride **4** is described according to its single-crystal X-ray structure. The spectrophotometric features (absorption and emission) of **1**, **2**, **3**, and **4** are reported along with the fluorescence response and affinity of **3** to some metal cations. The origin of the fluorescence from compounds **1** and **4** is investigated using density functional theory and the oscillator strength for each transition is computed. Two deactivation pathways, one of which is only weakly emissive, are identified in **4**. In contrast to **4**, which is only moderately more emissive than **1** a strong zinc-activated fluorescence response is observed from aqueous solutions of **3**.

Introduction

Fluorescent chemosensors are important tools for trace analyte detection in samples derived from biological or environmental sources. A variety of perspectives on the subject have appeared in recent review articles[1] and in very recent publications with a materials emphasis.[2] Many of the metal cation fluoroionophores operate through perturbation of photoinduced electron transfer, PET, processes resulting in fluorescence switching on or off as a consequence of metal binding at a receptor site on the sensor molecule.[3]

The fluorescence behavior of fluorogenic 8-hydroxyquinoline, 8-HQ, (also known as quinolinol and oxine) and its complexes and derivatives has been extensively and continually reported since the 1960s.[4] The 8-HQ compound is only weakly emissive, and this has recently been shown to be

* To whom correspondence should be addressed. E-mail: a.c.sullivan@qmul.ac.uk (A.S.); david.benoit@uni-ulm.de (D.M.B.).
[†] University of London.
[‡] University of Ulm.

(1) (a) Szacilowski, K.; Macyk, W.; Drzewiecka-Matuszek, A.; Brindell,; Stochel, G. *Chem. Rev.* **2005**, *105*, 2647. (b) de Silva, A. P.; Magri, D. C. *Chimia* **2005**, *59*, 218. (c) Martinez-Manez, R.; Sancenon, F. *J. Fluoresc.* **2005**, *15*, 267. (d) Prodi, L. *New, J. Chem.* **2005**, *29*, 31. (e) Rogers, C. W.; Wolf, M. O. *Coord. Chem. Rev.* **2002**, *233*, 350. (f) Zeng, Z. Y.; He, Y. B.; Meng, L. Z. *Prog. Chem.* **2005**, *17*, 265. (g) Bargossi, C.; Fiorini, M. C.; Montalti, M.; Prodi, L.; Zaccheroni, N. *Coord. Chem. Rev.* **2000**, *208*, 32. (h) Martinez-Manez; R.; Sancenon, F. *Chem. Rev.* **2003**, *103*, 4419.
(2) de Silva, A. P.; Tecilla, P. *J. Mater. Chem.* **2005**, *15*, 2637.
(3) (a) Rurack, K.; Resch-Genger, U. *Chem. Soc. Rev.* **2002**, *31*, 116. (b) Valeur, B.; Leray, I. *Coord. Chem. Rev.* **2000**, *205*, 3. (c). de Silva, A. P.; Fox, D. B.; Huxley, A. J. M.; Moody, T. S. *Coord. Chem. Rev.* **2000**, *205*, 41. (d). Prodi, L.; Bolletta, F.; Montalti, M.; Zaccheroni, N. *Coord. Chem. Rev.* **2000**, *205*, 59. (e) Gale, P. A. *Coord. Chem. Rev.* **2000**, *199*, 181. (f) Fabbrizzi, L.; Poggi, A. *Chem. Soc. Rev.* **1995**, *197*. (g) Bergonzi, R.; Fabbrizzi, L.; Licchelli, M.; Mangano, C. *Coord. Chem. Rev.* **1998**, *170*, 31. (h) Amendola, V., Fabbrizzi, L., Licchelli, M., Mangano, C.; Pallavicini, P.; Parodi L.; Poggi, A. *Coord. Chem. Rev.* **1999**, *190*, 0−192, 649. (i) Fabbrizzi, L.; Licchelli, M.; Pallavicini, P. *Acc. Chem. Res.* **1999**, *32*, 846. (j) Beer, P. D. *Acc. Chem. Res.* **1998**, *31*, 71. (k) de Silva, A. P.; Gunaratne, H. Q. N.; Gunnlaugsson, T.; Huxley, A. J. M.; McCoy, C. P.; Rademacher J. T.; Rice, T. E. *Chem. Rev.* **1997**, *97*, 1515.
(4) (a) Popovych O.; Rogers, L. B. *Spectrochim. Acta* **1959**, *27*, 584. Ohnesorge, W. E.; Rogers, L. B. *Spectrochim. Acta* **1959**, *27*, 27. (b) Ohnesorge, W. E.; Rogers, L. B. *Spectrochim. Acta* **1959**, *27*, 41. (c) Stevens, M. *Anal. Chim. Acta* **1959**, *20*, 389. (d) Popovych, O.; Rogers, L. B. *Spectrochim. Acta* **1960**, *28*, 49. (e) Lyttle, F. E.; Storey, D. R.; Juricich, M. E. *Spectrochim. Acta* **1973**, *29A*, 1357. (f). Dowling, H. S. D.; Seitz, W. R. *Spectrochim. Acta* **1984**, *40A*, 991. (g) Zhang, L. G.; Ren, X. G.; Jiang, P. D.; Lu, A. D.; Yuan, J. S. *Spectrosc. Lett.* **1996**, *29*, 995. (h) Ghasemi, J.; Shamsipur, M. *J. Coord. Chem.* **1992**, *26*, 337. (i) van Veldhoven, E.; Zhang, H.; Glasbeek, M. *J. Phys. Chem. A* **2001**, *105*, 1687.

10.1021/ic052085g CCC: $33.50
Published on Web 06/17/2006

Scheme 1 [a]

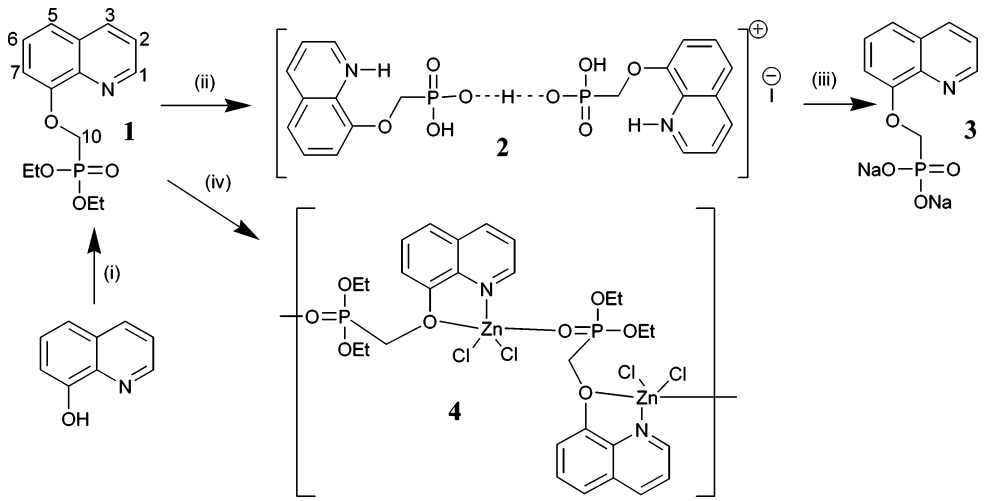

[a] (i) sodium hydride, diethyl-4-chlorophenylsulfonyloxymethylphosphonate. (ii) trimethylsilyl iodide, water; (iii) aqueous sodium hydroxide; (iv) $ZnCl_2$

due to photoexcited proton transfer, PPT, deactivation pathways.[5]

The 8-HQ as well as the 8-AQ (8-aminoquinoline) compounds have been extensively derivatized with metal-binding substituents with the aim of tuning the fluorescence response.[6−13] Functional groups that have been attached include 8-*p*-toluenesulfonamide, as in commercially available TSQ[6] and Zinquin,[7] dansyl,[8] ethylenediamine (in TQEN),[9] tris(2-aminoethyl)amine (in O-TRENSOX),[10] benzothiazole,[11] numerous crown ethers, for example, tri-thia-21-crown-7-ethers,[12] diaza-18-crown-6 ligands,[12] and tetraaza-crown ethers.[13]

We are interested in exploring the effects of the phosphonate group on both the chelating and fluorescence properties of 8-HQ. In this paper, we describe the synthesis, characterization, and spectrophotometric results for some new 8-quinolinyloxymethylphosphonate compounds. The quinoline chromophore has been featured in numerous studies focused on metal ion sensing that exploit PET and or photoinduced charge transfer, PCT.[6−9,14−17] Many of these reports feature work on selective sensing of zinc, owing to its considerable importance particularly in neurobiological processes. It is in this general context that we report here on our initial spectrophotometric studies of the 8-quinolinyloxymethylphosphonate compounds **1**, **4**, and **2** and some of its metal derivatives.

Results and Discussion

Synthesis and Characterization. Diethyl-8-quinolinyloxymethylphosphonate, 1. The 8-hydroxyquinoline phosphonate derivative **1** (Scheme 1) was synthesized by phosphonomethylation[18] of 8-hydroxyquinoline at the hydroxyl position using diethyl-4-chlorophenylsulfonylmethylphosphonate.

Compound **1** was purified by column chromatography and isolated in good yield as a tan-colored oil. It was characterized by ^{1}H, ^{13}C, and ^{31}P NMR spectroscopy (details given in the Experimental Section). The NMR assignments were confirmed by a combination of one- and two-dimensional experiments involving long-range (multiple bond) and short-range (single bond) $^{1}H-^{13}C$ correlation spectroscopy. The methylene protons at ArylOCH_2P are especially diagnostic, appearing as a doublet δ_H 4.64 ($J = 8.5$ Hz). The composition of **1** was further confirmed by the appearance of a molecular ion in the high-resolution mass spectrum at *m*/*z* 296.104.

In an attempt to convert **1** to the corresponding phosphonic acid using trimethylsilyl iodide, yellow crystals of the hemihydroiodide compound **2** were isolated. Compound **2** consists of cationic hydrogen-bonded dimeric units in the solid state (Figure 1a). A single peak was seen in the proton-decoupled ^{31}P spectrum of **2** at δ_P 15.42 considerably upfield

(5) Bardez, E.; Devol, I.; Larrey, B.; Valeur, B. *J. Phys. Chem. B* **1997**, *101*, 7786.
(6) Frederickson, C. J.; Kasarskis, E. J.; Ringo, D.; Frederickson, R. E. *J. Neurosci. Methods* **1987**, *20*, 91.
(7) Hendrickson, K. M.; Geue, J. P.; Wyness, O.; Lincoln, S. F.; Ward, A. D. *J. Am. Chem. Soc* **2003**, *125*, 3889.
(8) Jiang, P. J.; Chen, L. Z.; Lin, J.; Liu, Q.; Ding, J.; Gao, X.; Guo, Z. J. *Chem. Commun*. **2002**, 1424.
(9) Mikata, Y.; Wakamatsu, M.; Yano, S. *Dalton Trans.* **2005**, 545.
(10) Launay, F.; Alain, V.; Destandau, E.; Ramos, N.; Bardez, E.; Baret, P.; Pierre, J. L. *New J. Chem*. **2001**, *25*, 1269.
(11) Youk, J. S.; Kim, Y. H.; Kim, E. J.; Youn; N. J.; Chang, S. K. *Bull. Kor. Chem. Soc.* **2004**, *25*, 869.
(12) (a) Song, H. C.; Bradshaw, J. S.; Chen, Y. W.; Xue, G. P.; Li, W. M.; Krakowiak, K. E.; Savage, P. B.; Xu, Z. L.; Izatt, R. M. *Supramol. Chem.* **2002**, *14*, 263. (b) Su, N.; Bradshaw, J. S.; Zhang, X. X.; Song, H.; Savage, P. B.; Xue, G. P.; Krakowiak, K. E.; Izatt, R. M. *J. Org. Chem* **1999**, *64*, 8855. (c) Song, H. C.; Chen, Y. W.; Song, J. G.; Savage, P. B.; Xue, G. P.; Chiara, J. A.; Krakowiak, K. E.; Izatt, R. M.; Bradshaw, J. S. *J. Heterocycl. Chem.* **2001**, *38*, 1369.
(13) (a) Cui, X. L.; Cabral, M. F.; Costa, J.; Delgado, R. *Inorg. Chim. Acta* **2003**, *356*, 133. (b) Yang, Z. X.; Bradshaw, J. S.; Zhang, X. X.; Savage, P. B.; Krakowiak, K. E.; Dalley, N. K.; Su, N.; Bronson; R. T.; Izatt, R. M. *J. Org. Chem.* **1999**, *64*, 3162. (c) Xue, G. P.; Bradshaw, J. S.; Dalley, N. K.; Savage, P. B.; Krakowiak, K. E.; Izatt, R. M.; Prodi, L.; Montalti; M.; Zaccheroni, N. *Tetrahedron* **2001**, *57*, 7623. (d) Prodi, L.; Montalti, M.; Bradshaw, J. S.; Izatt, R. M.; Savage, P. B. *J. Incl. Phenom. Macrocyclic Chem.* **2001**, *41*, 123. Yasuoka, N.; Kasai, N. *Bull. Chem. Soc. Jpn.* **1985**, *58*, 1631.
(14) Fahrni, C. J.; O'Halloran, T. V. *J. Am. Chem. Soc.* **1999**, *121*, 11448.
(15) Kimber, M. C.; Geue, J. P.; Lincoln, S. F.; Ward, A. D.; Tiekink, E. R. T. *Aust. J. Chem.* **2003**, *56*, 39.
(16) Lim, N. C.; Freake, H. C.; Bruckner, C. *Chem. Eur. J.* **2004**, *11*, 38.
(17) Jiang, P. J.; Guo, Z. J. *Coord. Chem. Rev.* **2004**, *248*, 205.
(18) Cornforth, J. W.; Wilson, J. R. H. *J. Chem. Soc., Perkin Trans.* **1994**, *1*, 1897.

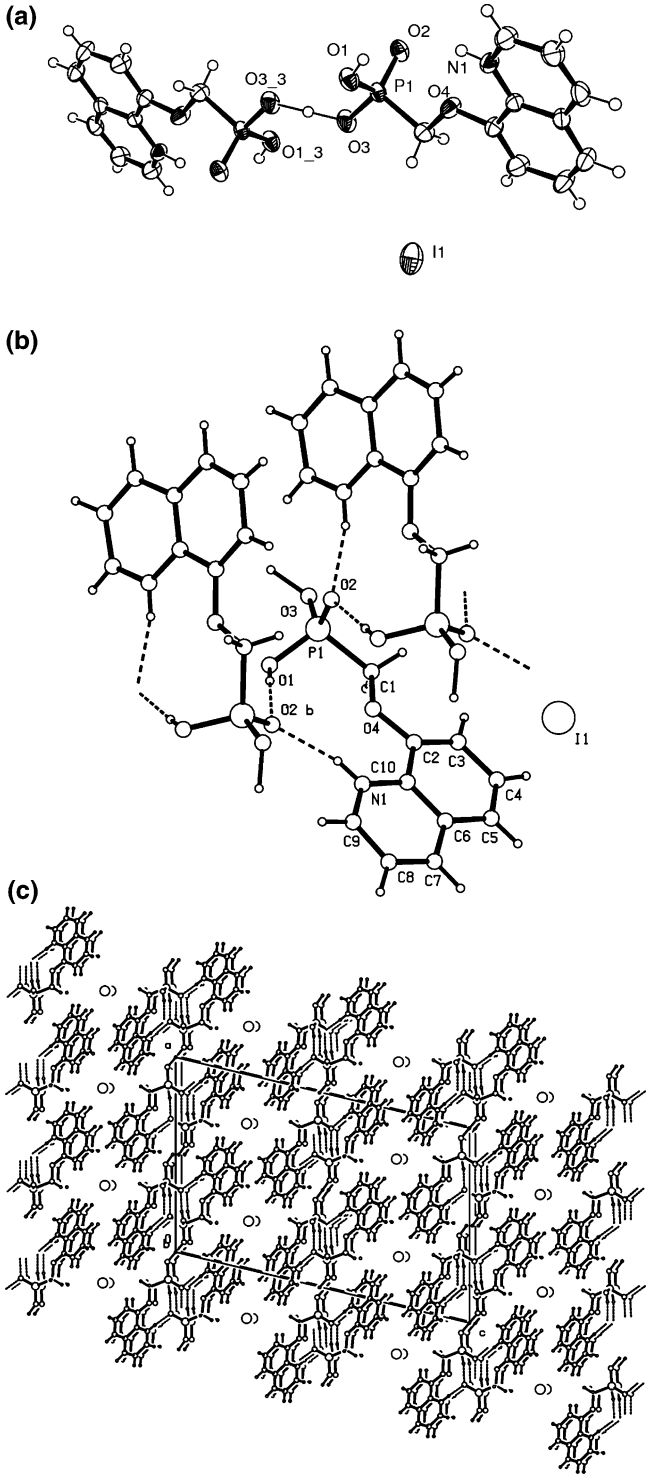

Figure 1. (a) Solid-state structure of **2**. (b) Hydrogen bonding in **2**. (c) Packing diagram for **2** (along the *b* axis).

from that observed for **1**. The doublet resonance for the methylene protons δ_H 5.34, ArylOCH_2P, is downfield of that in **1**. The spectra suggest that the 1:2 HI/phosphonic acid compound **2** does not reorganize to form a mixture of the discrete 1:1 species and phosphonic acid in solution. Solutions of **3** that we will refer to as solutions of the disodium phosphonate, were prepared upon addition of 2.5 equiv of NaOH to solutions of hemihydroiodide **2**. The 1:1 adduct **4** between compound **1** and zinc chloride [$ZnCl_2$] was formed when **1** and the metal compound were combined in diethyl ether. Single crystals of the product were isolated in moderate yield after recrystallization of the crude material from ethanol. NMR data for **4** reveal only slight chemical shift differences relative to **1**. In particular, the ^{31}P resonance is shifted ~1 ppm from 21.46 to 22.6 ppm in the zinc complex.

The bulk composition of **4** was confirmed by elemental analyses. The solid-state structure was determined by single-crystal X-ray diffraction and is discussed below.

Crystallography. Compound 2. The structure of compound **2** is shown in Figure 1 with selected bond distances and angles in Table 1 and crystal data in the Experimental Section. Hydrogen bonding is summarized in Table 2. The simplest representation, Figure 1a, of the structural unit consists of a cationic hydrogen-bonded quinolinium pair with (P)O···H−O(P) and N−H···O(P), as well as N−H···(OH)P, bonds and a discrete iodide anion (hydrogen bond distances are in Table 2). In the extended structure, Figure 1b, additional intermolecular chain-forming hydrogen bonds of the type (P)O−H−O(P) are evident. These interactions ultimately generate a 3-dimensional assembly of stacked chains that define channels where the stacked iodide ions are accommodated, Figure 1c. The ring-to-ring distance in the stacked structure is 5.513 Å. The P−OH and P═O distances are clearly discriminated, for example, P(1)−O(1) = 1.560(2) Å and P(1)−O(2) = 1.492(2) Å.

Compound 4. The solid-state structure of compound **4** is shown in Figure 2 with selected bond distances and angles in Table 1 and crystal data in the Experimental Section. The geometry at zinc is very distorted trigonal-bipyramidal with the base of the pyramid comprising the quinoline nitrogen and the two chlorine atoms, Figure 2a. The apical positions are occupied by the oxygen of the quinolinoxy fragment and a phosphonyl oxygen from a neighboring phosphonate group. The bond distances associated with quinolinoxy chelation, Zn(1)−O(1) and Zn(1)−N(1) in **4** 2.4898(14) and 2.0697(15) Å, respectively, are longer (particularly the former) than those, 2.176(4) and 2.047(4) Å, respectively, in anhydrous zinc quinolinate.[19] The Zn−O(P) distance, 2.0693(14) Å, is markedly shorter than Zn−$O_{quinolinoxy}$, signifying a stronger bond. The phosphonate groups act as linkers between adjacent molecules, leading to chains that are arranged such that the quinolinoxy fragments form stacked columns, Figure 2b.

Spectrophotometric (Absorption and Fluorescence) Studies. Compound 1. The concentration-dependent absorption and fluorescence (λ_{ex} = 311 nm, λ_{em} = 388 nm) spectra of **1** are shown in Figures 3 and 4. Absorption peaks close to 300 nm have previously been assigned to n−π* and π−π*, and transitions for the parent oxine compound[4g] and more recently to π−π* in experimental and theoretical studies of the tris(quinolinato)aluminum compound.[4i] Compound **1** is observed to be more fluorescent than the parent oxine, presumably due to the absence of PPT-forming nonradiative tautomers.

(19) (a) Palenik, G. J. *Acta Crystallogr.* **1964**, *17*, 696. (b) Kai, Y.; Morita, M.; Yasuoka, N.; Kasai, N. *Bull. Chem. Soc. Jpn.* **1985**, *58*, 1631.

Table 1. Selected Bond Distances (Å) and Angles (deg)

compound **2**		compound **4**		compound **2**		compound **4**	
P(1)−O(2)	1.492(2)	Zn(1)−N(1)	2.0697(15)	O(2)−P(1)−O(3)	116.10(12)	O(2)−P(1)−O(3)	162.14(5)
P(1)−O(3)	1.517(2)	Zn(1)−O(1)	2.4898(14)	O(2)−P(1)−O(1)	112.58(13)	N(1)−Zn(1)−O(2)	93.57(6)
P(1)−O(1)	1.560(2)	Zn(1)−O(2)	2.0693(14)	O(3)−P(1)−O(1)	107.51(13)	N(1)−Zn(1)−Cl(2)	111.20(5)
P(1)−C(1)	1.803(3)	Zn(1)−Cl(2)	2.2240(8)	O(2)−P(1)−C(1)	109.16(15)	O(2)−Zn(1)−Cl(1)	97.46(4)
		Zn(1)−Cl(1)	2.2389(8)	O(3)−P(1)−C(1)	105.09(14)	O(2)−Zn(1)−Cl(2)	104.97(4)
		O(2)−P(1)	1.4735(14)	O(1)−P(1)−C(1)	105.65(15)	N(1)−Zn(1)−Cl(1)	124.91(5)
		O(3)−P(1)	1.5406(17)			Cl(2)−Zn(1)−Cl(1)	117.40(3)
		O(4)−P(1)	1.5466(17)			P(1)−O(2)−Zn(1)	138.40(9)
		P(1)−C(7)	1.799(2)			C(11)−O(3)−P(1)	126.0(2)
						C(13)−O(4)−P(1)	126.05(17)
						O(2)−P(1)−O(3)	112.46(9)
						O(2)−P(1)−O(4)	115.62(9)
						O(3)−P(1)−O(4)	105.14 (9)
						O(2)−P(1)−C(7)	110.48(9)
						O(3)−P(1)−C(7)	107.65(9)
						O(4)−P(1)−C(7)	104.91(9)

Table 2. Hydrogen Bonds for **2** (Å and deg)[a]

D−H···A	*d*(D−H)	*d*(H···A)	*d*(D···A)	<(DHA)
N(1)−H(1N)···O(2) (1)	0.87(3)	1.93(4)	2.780(3)	166(3)
O(1)−H(1O)···O(2) (1)	0.82(4)	1.84(4)	2.651(3)	172(4)
O(3)−H(3O)···O(3) (2)	1.212(2)	1.212(2)	2.424(4)	180.0(3)

[a] Symmetry transformations used to generate equivalent atoms: 1, $-x + 1/2, y + 1/2, -z + 0$; 2, $-x, -y, -z$.

Compound 4. The absorption and fluorescence spectra of **4** are shown in Figures 5 and 6. There is little change in the absorption spectrum relative to **1**, but the emission in **4** is slightly red-shifted and the intensity is enhanced with respect to **1**. The enhancement as shown in Figure 6, ∼174%, is a slight underestimate since the spectra are not normalized to take account of the slightly larger molar absorptivity of **1** at the excitation wavelength 318 nm **4** (3700 and 2500 M^{-1} cm^{-1} for **1** and **4**, respectively). The enhancement is small compared to that seen for many zinc sensors and shows that cancellation of any emission-quenching PET due to the nitrogen lone pair has a relatively small effect on emission intensity in this case. The percentage enhancement is, however, of the order predicted theoretically for this system (see below).

The observed emission behavior from **1** and its zinc compound **4** were predicted by a computational study where we compared the fluorescence emission process for compound **1** and a model of compound **4** (see Computational Details). To investigate the fluorescence behavior of these compounds, we focus on the lowest energy transition from the singlet excited state (S_1) to the electronic ground state (S_0). A selection of optimized M−L bond lengths for the model of compound **4** in both its electronic ground state (S_0) and its first singlet excited state (S_1) are shown in Table 3. The computed bond lengths for S_0 are in qualitative agreement with the X-ray data measured on the polymeric crystal. In particular, we note that the Zn−Cl distances and the Zn−N distance are in very good agreement with experiment, while the Zn−O distances are too short in our model. However, in the polymeric crystal, the oxygen atoms are acting as structural bridging elements which account for the deviation from our computational model. We note that in both our model and the experimental data, the zinc center is in a slightly distorted trigonal-bipyramidal geometry. Upon excitation to S_1, the complex does not undergo any significant distortion apart from a slight change in the Zn−O distances and in the O−Zn−O angle, which results in the overall geometry of the zinc center being closer to an ideal trigonal-bipyramid (see Table 3).

We see in Table 4 that the observed fluorescence emission band of compound **1** at 390 nm is well reproduced, with a difference between the calculated and measured transition energy smaller than 0.1 eV. The emission transition of compound **4** at 400 nm is not as successfully reproduced, but with an error in the transition energy close to 0.4 eV, our computed value remains within the usual accuracy of time-dependent density functional theory (TDDFT) for this type of system.

The relative intensity of these transitions is related to the magnitude of the change in dipole moment, which is shown in Table 4 and graphically in Figure 7. If we take as a reference the magnitude of the dipole change for the $S_1 \rightarrow S_0$ transition of compound **1**, we note that the same transition for compound **4** is predicted to be more intense (131%).

The origin of this theoretical enhancement of fluorescence activity can be understood by looking at the change in electronic density that occurs during the fluorescence transition (Figure 7). Compound **1** undergoes a transition that shifts electronic density from one side of the fluorophore to the other (see Figure 7A), characteristic of a $\pi^* \rightarrow \pi$ transition. Instead, compound **4** sees its electron density being shifted in a different direction toward p orbitals located on the chlorine atoms (see Figure 7B), thus exhibiting a transition similar to an $\pi^* \rightarrow$n de-excitation. In this compound, the zinc atom acts as a mediator between the bi-cycle and the halogen ligands and, due to its direct bonding with the lone-pair of the nitrogen atom in the bi-cycle, opens a de-excitation pathway that was closed for compound **1**.

Our TDDFT results (see Table 4) show that a second de-excitation channel exists for compound **4**. The de-excitation process $S_2 \rightarrow S_0$ (see Figure 7C) looks similar to the $S_1 \rightarrow S_0$ process for compound **1** since the electron density is shifted from one side of the fluorophore to the other with a similar change in dipole moment. The presence of this second channel at a similar energy to $S_1 \rightarrow S_0$ suggests that the fluorescence emission could occur through a combination of a metal-mediated $\pi^* \rightarrow$n emission and a fluorophore-based

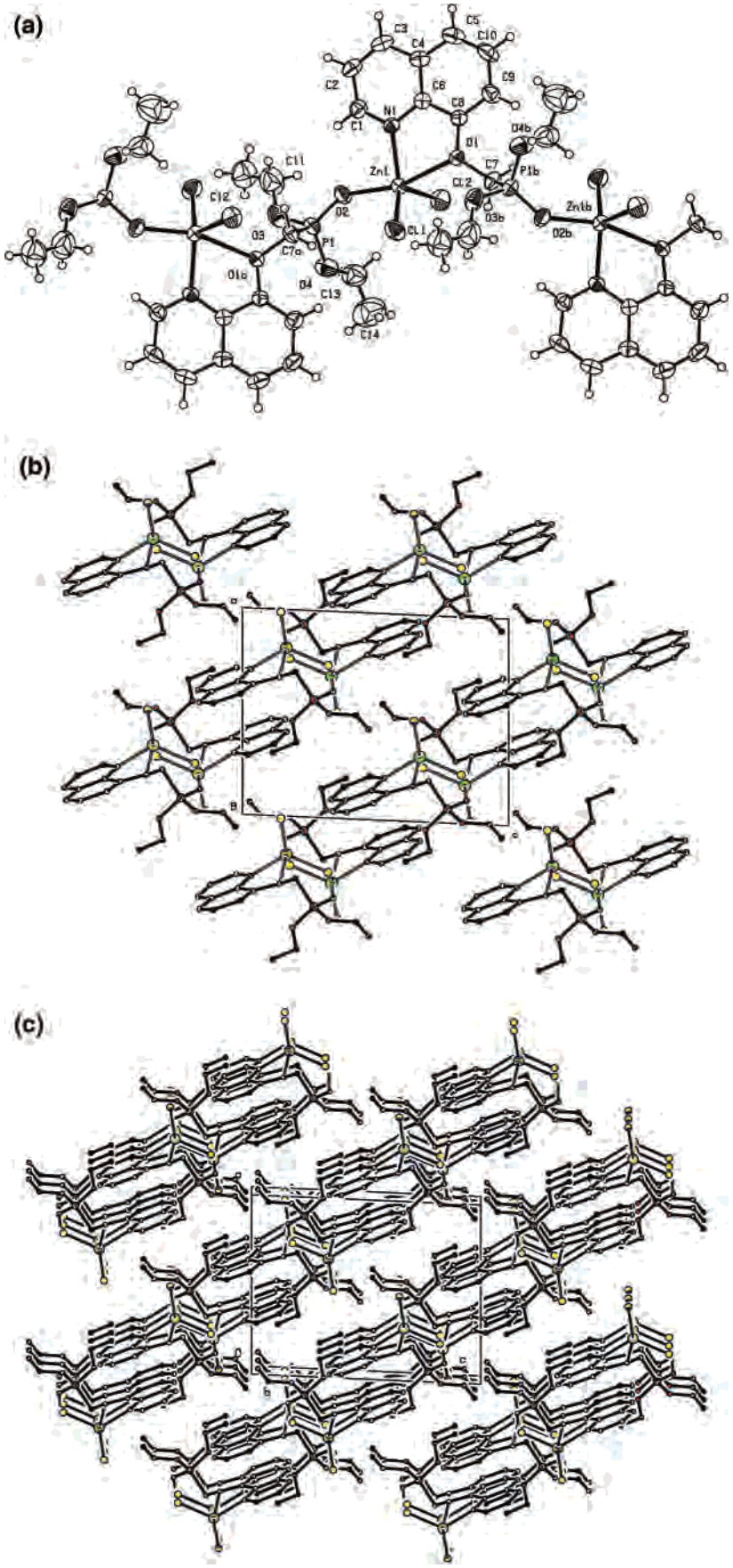

Figure 2. Packing in **4** (hydrogen atoms are omitted; along the *b* axis showing stacking).

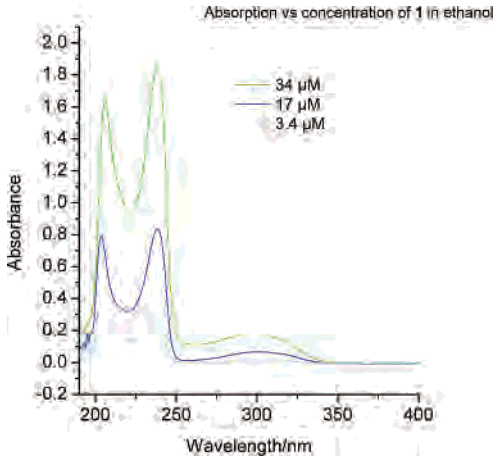

Figure 3. Absorption spectra of **1** in ethanol (3.4, 17, 34 μM).

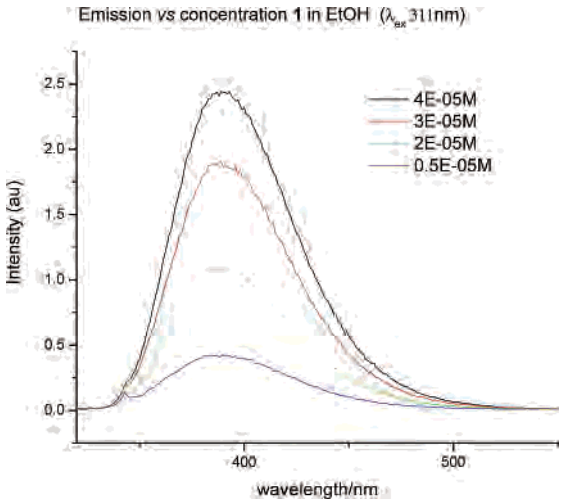

Figure 4. Emission spectra of **1** in ethanol (5, 20, 30, 40 μM).

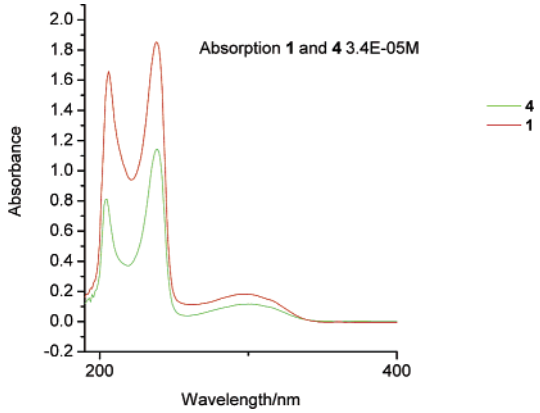

Figure 5. Comparison between absorption spectra of **1** and **4** (in ethanol 34 μM).

$\pi^*\rightarrow\pi$ emission as seen in compound **1**. An analysis of the computed oscillator strength shown in Table 4 shows that the first channel ($S_1\rightarrow S_0$ transition) is expected to be about 3 times weaker than the second de-excitation channel ($S_2\rightarrow S_0$ transition). This is consistent with the nature of each transition, since the second channel is closer in character to a pure fluorophore $\pi^*\rightarrow\pi$ transition and thus should be more radiative than the new zinc-mediated channel which involves mainly nonbonded chlorine orbitals.

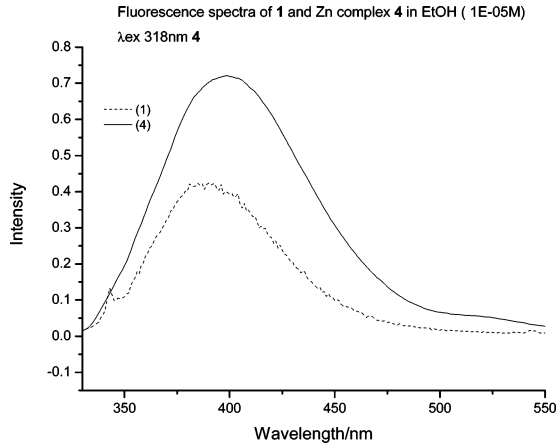

Figure 6. Comparison between emission spectra of **1** and **4** (in ethanol 10 μM).

Table 3. Selected Distances (Å) and Angles (deg) for the Electronic Ground State and First Singlet Excited State of Compound **4**[a]

distance	LDA (S_0)	exptl	LSE/LDA (S_1)
Zn−Cl(1)	2.201	2.2390(8)	2.191
Zn−Cl(2)	2.201	2.2237(7)	2.209
Zn−O(1)	2.262	2.4901(15)	2.319
Zn−O_w(2)	2.266	2.0698(14)	2.190
Zn−N(1)	1.990	2.0695(15)	1.949
Cl(1)−Zn−Cl(2) (α)	118.2°	117.40(3)	118.1°
O(1)−Zn−O_w(2) (β)	168.9°	162.14(5)	175.2°
$\tau = (\beta - \alpha)/60°$	0.85	0.75	0.95

[a] O_w denotes the oxygen atom of the water molecule. The degree of trigonality, τ, goes from 0 for a tetragonal geometry to 1 for a trigonal-bipyramidal geometry.[27]

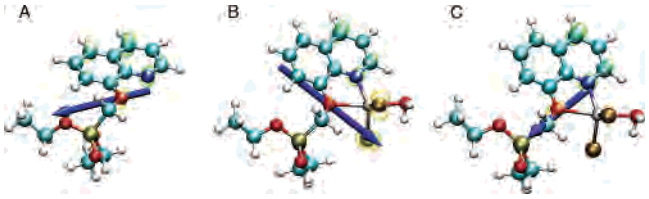

Figure 7. Density difference plot for compounds (A) **1** and (B−C) **4** at their respective optimized geometries in the S_1 state. The electronic density shifts from the green region to the yellow region upon $S_1\rightarrow S_0$ de-excitation for A and B and $S_2\rightarrow S_0$ for C. The blue arrows show the change in dipole moment for each transition.

The availability of this weakly emissive deactivation pathway may account for the smaller-than-expected enhancement due to PET cancellation in the zinc complex of **1**.

Compound 2 and Its Derivatives. The absorption and concentration dependent fluorescence spectra of **2** are shown in Figures 8 and 9. For aqueous **2** (34μM, pH 4.2), absorption in the 300 nm region is weak compared to **1**, probably as a consequence of protonation at the quinolinoxy nitrogen (Figure 8). The major species under these conditions is assumed to be the N-protonated monoanion. Further deprotonation to the phosphonate dianion by addition of NaOH can be followed by the decrease of λ_{max} 250 nm and growth of λ_{max} 240 nm with an isosbestic point at 244 nm (Figure 8 and Scheme 2). The pK value 5.1 was evaluated using fractional composition versus pH analysis. The emission maximum (Figure 9) is slightly red-shifted with dilution (probably due to small changes in pH).

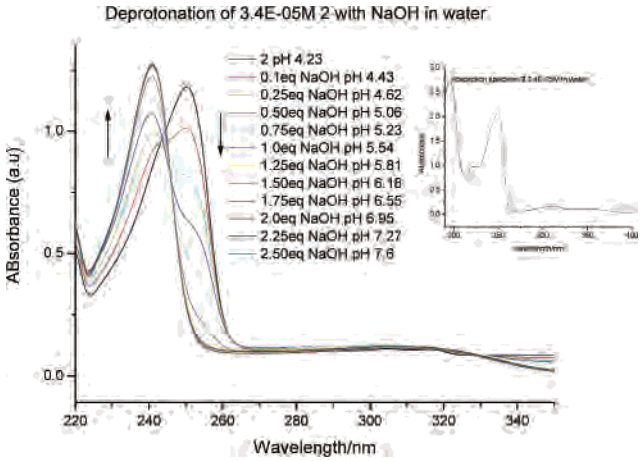

Figure 8. Deprotonation titration profile for **2** (34 μM) with NaOH; initial pH 4.2 and at 2.5 equiv of NaOH added pH 7.6; pK 5.1 for equilibrium observed (by fractional composition vs pH analysis). Inset: absorption spectrum of aqueous 34 μM **2**.

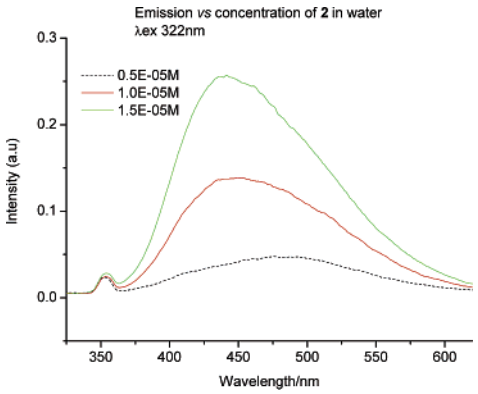

Figure 9. Emission spectra of aqueous **2** (5, 10, 15 μM).

The absorption band at 300 nm is once again evident after addition of 2.5 equiv of NaOH to solutions of **2** to give solutions **3** of the disodium phosphonate. (Figure 10). Two-fold fluorescence enhancement is seen on formation of **3** from **2** (Figure 11).

The fluorescence response from 5 μM **3** to zinc showed an 11-fold enhancement with respect to **3** (baseline fluorescence measured in the absence of any added chelator such as TPEN or EGTA) (Figure 12a). This response is more in line with that of other zinc-activated fluorescence probes with quinoline chromophores such as TSQ or Zinquin.[6−8,16] Titration of **3** with Zn^{2+} resulted in a decrease in the band at 240 nm, isosbestic points at 235 and 245 nm, and a slight change in the shape of the band 260−360 nm close to 315 nm (see insets Figure 12a). There was no change in pH after the addition of 2 equiv of Zn^{2+} to 34 μM **3**. The emission titration spectra for Zn, Ca, Mg, and Cu are shown in Figure

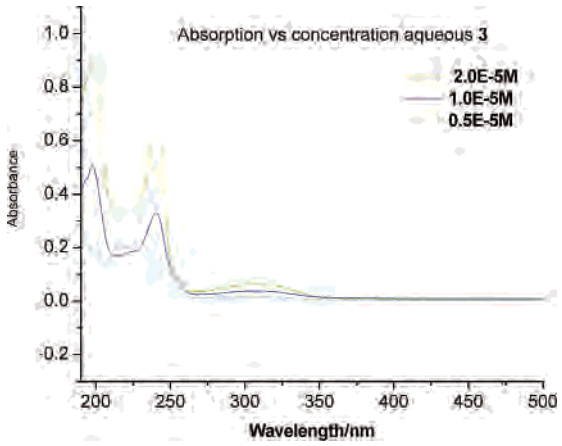

Figure 10. Absorption spectra of **3** (in water 5, 10, 20 μM).

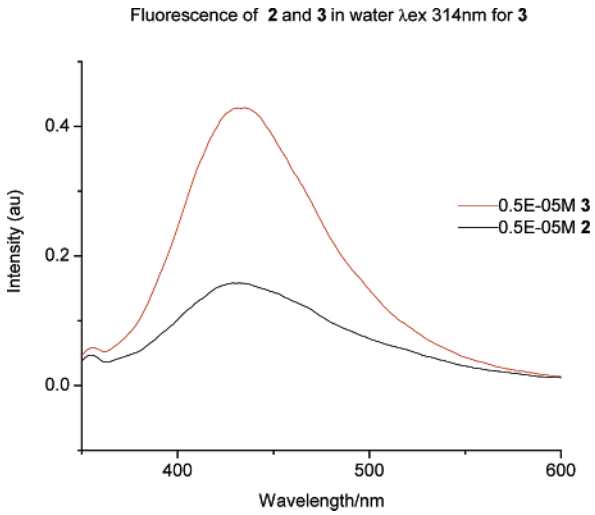

Figure 11. Comparison between emission spectra **2** and **3** (in water 5 μM).

Scheme 2

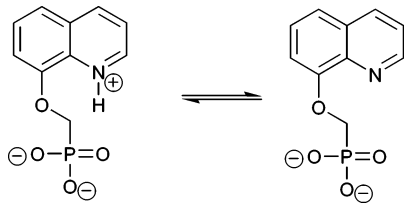

12a−d. Nonlinear fitting of the emission titration profiles to the quadratic based on 1:1 complexation gave equilibrium association constants $K = 2 \times 10^6$ (Zn), 2×10^6 (Ca), and 4.6×10^6 M^{-1} (Mg). The fluorescence response of 5 μM **3** to various metal ions is shown in Figure 13. There is an 11-fold enhancement for zinc, a 7-fold enhancement for calcium, and much weaker responses for magnesium and

Table 4. Transition Energies, Magnitude of Dipole Change, Oscillator Strength, and Nature of Transitions for the Fluorescence Process of Compounds **1** and **4**

compound		transition energy (eV)		dipole magnitude (D)	oscillator strength	nature of transition
		TDDFT	exptl			
1	$S_1 \rightarrow S_0$	3.10 (400 nm)	3.18 (390 nm)	15.8 (100%)	0.1176	87% (LUMO→HOMO)
4	$S_1 \rightarrow S_0$	2.71 (458 nm)	3.10 (400 nm)	20.7 (131%)	0.0192	82% (LUMO→HOMO−1) 15% (LUMO→HOMO)
	$S_2 \rightarrow S_0$	2.73 (454 nm)	16.7 (106%)		0.0649	17% (LUMO→HOMO−1) 68% (LUMO→HOMO)

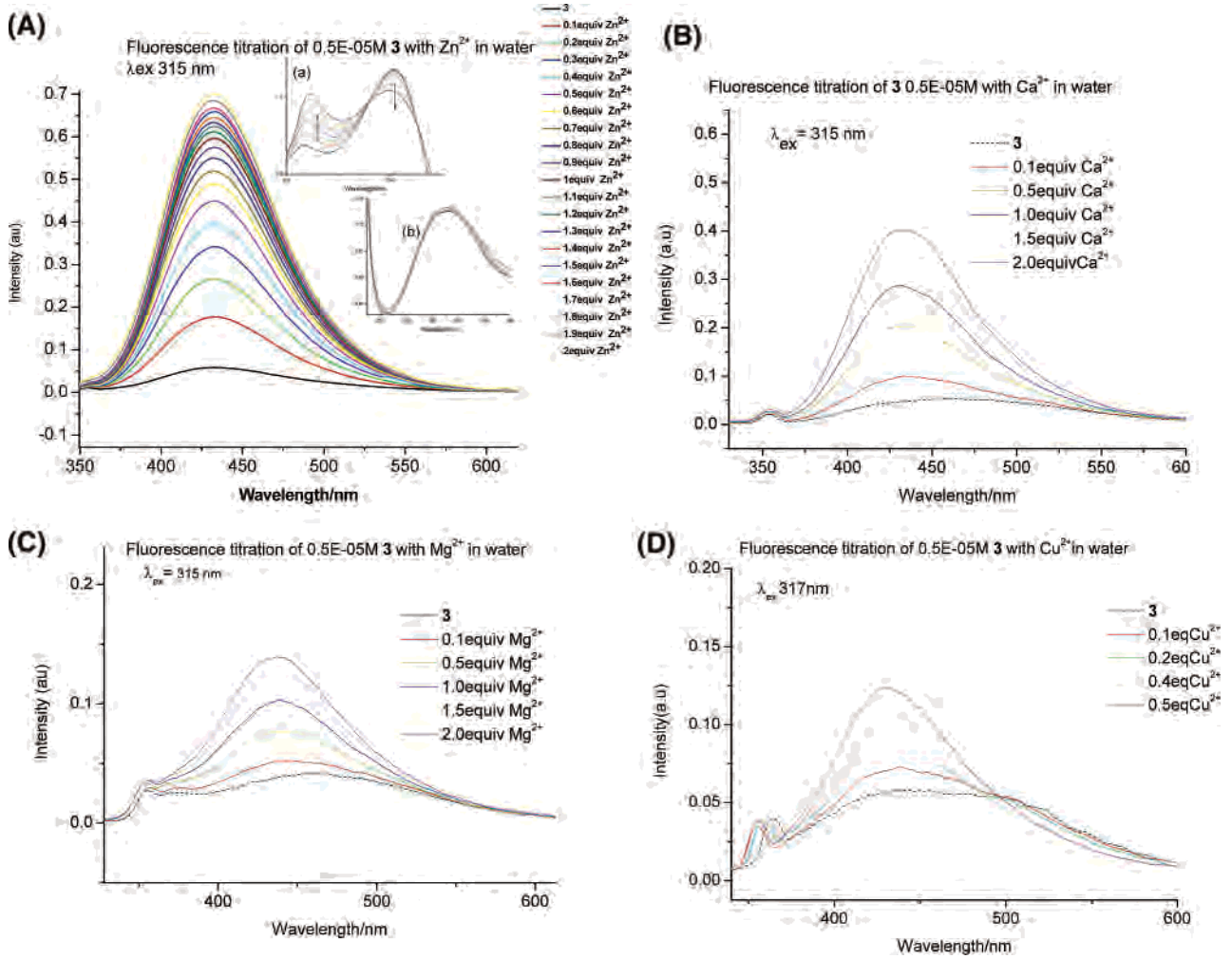

Figure 12. (A) Emission spectra showing the titration of aqueous 5 μM **3** with aqueous zinc nitrate. Inset (a) absorption spectra 220−250 nm for titration of 34 μM **3** with Zn^{2+} and (b) absorption 260−360 nm for titration of 34 μM **3** with Zn^{2+}. (B) Emission spectra showing titration of aqueous 5 μM **3** with aqueous calcium nitrate. (C) Emission spectra showing titration of aqueous 5 μM **3** with aqueous magnesium chloride. (D) Emission spectra showing titration of aqueous 5 μM **3** with aqueous cupric nitrate (quenching observed above 0.5 equiv of Cu^{2+}).

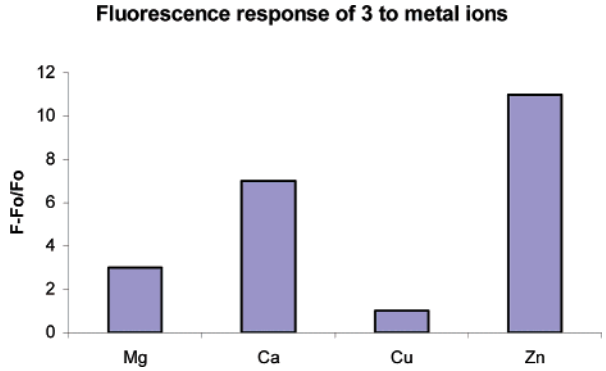

Figure 13. Fluorescence response of aqueous solutions 5 μM in **3** and 10 μM in divalent metals (Mg, Ca, Zn) and 2.5 μM Cu.

copper. Solutions which are 5 μM **3** and up to 2.5 μM in copper gave a slightly enhanced response, but quenching of the signal was observed at higher concentrations of copper. We observed that the weakly fluorescent 5 μM aqueous 8-HQ parent showed no response when titrated with Ca^{2+}. Others have reported a decrease in association constants for the 8-HQ/Ca^{2+} system on going from acetonitrile ($K = 10^3$ M^{-1}) to methanol ($K = 10^2$ M^{-1}).[4h] Overall, our results indicate that useful metal-activated sensing can be expected from solutions of disodium phosphonate **3**. The fluorescence response of **3** to zinc indicates that deactivation pathways associated with **1** are absent here and this may be associated with zinc ligand (nitrate in this case) displacement by the phosphonate dianion. Further work on the structural chemistry of metal derivatives of **2** and related compounds is in progress, and this will be reported along with more detailed spectrophotochemical, theoretical, and coordination chemistry studies in due course.

Conclusions

Methylphosphonate derivatives of 8-hydroxyquinoline, including diethyl 8-quinolinyloxymethylphosphonate **1** and 8-quinolinyloxymethylphosphonic acid hemihydroiodide **2**, have been synthesized and characterized. Solutions of the disodium methylphosphonate derivative **3** were prepared and used in situ from solutions of **2** and sodium hydroxide. Compound **1** forms a 1:1 chain polymeric compound **4** with zinc chloride. The spectrophotometric features show emission intensity varies as **1** ≈ **2** < **3**, and both **2** and **3** are red-shifted relative to **1**. Compound **4** is red-shifted and more

fluorescent than **1**. The computational study predicts enhanced fluorescence in the zinc chloride complex. This interaction, however, opens up a new weakly emissive pathway through which the electron density is shifted toward the halogen ligands of the metal. The latter may account for the smaller-than-expected enhancement due to PET cancellation in the zinc complex of **1**. The emission of 5 μM **3** in water shows 11-fold enhancement with added zinc. Smaller enhancements are seen for 5 μM **3** and 2 equiv of added calcium ($\sim\times 7$) or magnesium ($\sim\times 3$) or 0.5 equiv of added copper ($\sim\times 2$). To our knowledge, phosphonate groups have not previously been employed as receptors in PET sensors. We are currently investigating the coordination chemistry, in both the solid state and the solution phase, for this system. More detailed studies (structural and spectrophotometric) on metal derivatives of **1** and **2** and other phosphonomethylated emissive systems will be reported in forthcoming papers.

Experimental Section

The solvents DMSO and DCM were dried over and distilled from molecular sieves and calcium hydride, respectively, and subsequently stored over molecular sieves.

Reagents and spectroscopic grade solvents were purchased from Aldrich, Lancaster, Fluka, or Avocado and were used without further purification.

NMR spectra were recorded on JEOL 270, Bruker AM250, and AMX600 spectrometers. The chemical shifts are reported in parts per million (ppm) relative to the position of the solvent signal, and numbering refers to the positions indicated for **1** in the scheme. The chemical shifts (δ) for the solvents are, $CDCl_3$ (^{1}H, 7.26; ^{13}C, 77.23), CD_3OD (^{1}H, 4.87; ^{13}C, 49.15), and DMSO-d_6 (^{1}H, 2.50; ^{13}C, 39.50). Infrared spectra were recorded on a Perkin-Elmer FTIR 1720X spectrometer equipped with an ATR (attenuated total reflectance) attachment in the range of 4000−400 cm^{-1}. Mass spectra were obtained from services at the School of Pharmacy, London, and the EPSRC Mass Spectrometry service at the University of Swansea.

Elemental analyses (carbon, hydrogen, nitrogen) were obtained from services at University College London. Melting points were observed on an Electrothermal melting point apparatus.

UV−vis spectra were recorded on a Hewlett-Packard 845x UV−visible system equipped with a deuterium and tungsten lamp with 1 cm quartz cells at room temperature. The pH of solutions was measured using a Hanna HI 8424 pH meter.

Fluorescence spectra were obtained from a Yvon Jobin Fluoromax 3 instrument. The spectrophotometric titrations (uncorrected for performance of the instrument) were performed by addition of millimolar aqueous metal ion solutions in 2.5 μL aliquots to 5 μM **1** or **3**. The change in concentration of **1** or **3** was assumed to be negligible.

Preparation of Diethyl 8-Quinolinyloxymethylphosphonate, 1. A solution of 8-hydroxyquinoline (2.90 g, 20 mmol) in dry dimethyl sulfoxide (15 cm^3) was added to dry 40−60 petrol-washed sodium hydride (0.83 g, 21 mmol) to give a yellow solution. When the initial reaction had subsided, the reaction mixture was stirred at room temperature for 1 h. A solution of diethyl-4-chlorophenylsulfonyloxymethylphosphonate (7.2 g, 21 mmol) in dry dimethyl sulfoxide (30 cm^3) was added, and the mixture stirred under nitrogen for 96 h at room temperature. The mixture was then diluted with water (50 cm^3), and ethyl acetate (150 cm^3) was added. The organic layers were extracted and washed with brine (3 × 50 cm^3) then dried over magnesium sulfate. Ethyl acetate was removed under reduced pressure to give a dark green-brown oil. The oil was purified by chromatography on silica using petroleum ether/ethyl acetate 9:1 followed by 2:8 petroleum ether/ethyl acetate containing approximately 5% methanol to elute the product. The solvent was removed under reduced pressure to give diethyl-8-quinolinyloxymethylphosphonate as a brown oil with a yield of 62% based on 8-hydroxyquinoline. MS(FAB MNOBA matrix) *m*/*z* 296.104; *m*/*z* calcd for $C_{15}H_{19}NO_4P$ 296.105 [MH$^+$]. ^{1}H NMR (600 MHz, CD_3OD) δ 8.72 (1H, dd, J_1 5.8 Hz, J_2 1.6 Hz, H_1), 8.19 (1H, dd, J_1 9.8 Hz, J_2 1.5 Hz, H_3), 7.44 (1H, dd, J_1 9.8 Hz, J_2 1.3 Hz, H_5), 7.42 (1H, t, *J* 4.3 Hz, H_2), 7.41 (1H, t, *J* 1.7 Hz, H_6), 7.28 (1H, dd, J_1 8.5 Hz, J_2 1.2 Hz, H_7), 4.64 (2H, d, *J* 8.4 Hz, H_{10}), 4.17 (4H, dt, J_1 7.1 Hz, J_2 7.0 Hz, H_{11}), 1.23 (6H, t, *J* 7.1 Hz, H_{12}). ^{13}C{^{1}H} (150.92 MHz, CD_3OD) δ 155.25 (d, J_{C-P} 9.2 Hz, C_8), 150.25 (C_1), 140.99 (C_9), 137.85 (C_3), 131.09 (C_4), 127.92 (C_6), 123.06 (C_2), 122.42 (C_5), 112.26 (C_7), 64.53 (d, J_{C-P} 6.8 Hz, C_{11}), 64.00 (d, J_{C-P} 166.9 Hz, C_{10}), 16.74 (d, J_{C-P} 5.8, C_{12}). ^{31}P{^{1}H} δ (242.94 MHz, CD_3OD) 21.46. IR (cm^{-1}): 2983w, 1571m, 1500m, 1471w, 1377w, 1318w, 1245m (P═O), 1112m (C−O), 1022s (P−O−C), 973m (P−O), 824w, 530s, 492s.

Preparation of 8-Quinolinyloxymethylphosphonic Acid Hemihydroiodide, 2. To a stirred solution of **1** (0.92 g, 3.12 mmol) dissolved in dry dichloromethane (16 cm^3) under an atmosphere of nitrogen was added trimethylsilyl iodide (1.8 cm^3). The red solution was stirred for 2 h, and then methanol (25 cm^3) was added. After 2 h, the solvent was removed under reduced pressure and then water (20 cm^3) was added to the residue. The mixture was concentrated under reduced pressure. This was repeated four times to give yellow needles of **2** with a yield of 94% based on **1**. mp = 285−288 °C. Anal. Found: C, 39.34;H, 3.51;N, 4.43. Calcd for $C_{10}H_{11}I_{0.5}NO_4P$: C, 39.62;H, 3.49;N, 4.62. ^{1}H NMR (600 MHz, DMSO-d_6) δ 11.39 (2H, bs, N*H*), 9.89 (1H, d, *J* 3.4 Hz, H_1), 9.50 (1H, d, *J* 8.3 Hz, H_3), 8.63 (1H, dd, J_1 4.5 Hz, J_2 3.4 Hz, H_2), 8.53 (2H, m, H_6 and H_7), 8.39 (1H, bd, *J* 7.3 Hz, H_5), 5.34 (2H, d, *J* 9.6 Hz, H_{10}). ^{13}C{^{1}H} NMR (150.92 MHz, DMSO-d_6) δ 152.59 (d, J_{C-P} 12.1 Hz, C_8), 147.45 (C_1), 139.54 (C_9), 135.66 (C_3), 129.08 (C_4), 127.87 (C_6), 122.09 (C_2), 120.34 (C_5), 111.63 (C_7), 64.92 (d, J_{C-P} 161.4 Hz, C_{10}). ^{31}P{^{1}H} (242.94 MHz, DMSO-d_6) δ 15.42. IR (cm^{-1}) 2754bw (OH), 1635w, 1597m (C═C), 1556s, 1417s (C═C), 1396m, 1304s (P═O), 1267m, 1214m, 1002s (P−OH), 937s (P−OH), 819s, 758s, 715s, 615s, 605s, 520s, 474s. MS (CI negative ion mode, NH_3) *m*/*z* 239; *m*/*z* calcd for $C_{10}H_{10}NO_4P$ 239.1 (M − HI).

Quantum yield, $\phi_2 = 0.67$ (with respect to anthracene as standard where $\phi_{ant} = 0.27$) by standard method described on Jobin Yvon website literature.[22]

Stock solutions of **2** 0.01 M in either DMSO or ethanol were diluted in water. Solutions of **3** were prepared by addition of 2.5 equiv of aqueous millimolar NaOH to millimolar hemi hydroiodide **2** with subsequent dilution as required.

Preparation of 1·$ZnCl_2$, 4. To a suspension of zinc dichloride (0.24 g, 1.76 mmol) in dry ether (20 cm^3) was added a solution of 8-quinolinyloxymethylphosphonate (0.47 g, 1.59 mmol) in dry ether (10 cm^3) to form a white precipitate. The mixture was left to stir under an atmosphere of nitrogen at room temperature for 48 h. The solvent was removed under vacuum, and the precipitate was

(20) Yvon, J. *A guide to recording Fluorescence Quantum Yields*; www.jobinyvon.com.
(21) Enraf-Nonius *CAD-4/PC*, Version 1.5c; Enraf-Nonius: Delft, The Netherlands, 1994.
(22) North, A. C. T.; Phillips, D. C.; Mathews, F. S. *Acta Crystallogr. Sect. A* **1968**, *42*, 351.

recrystallized from ethanol to give colorless crystals with a yield of 44% based on **1**. mp = 170−177 °C. Anal. Found: C 38.96; H 4.12; N 3.16. Calcd for $C_{14}H_{18}Cl_2NO_3PZn$: C 38.96; H 4.20; N 3.25. ^{1}H NMR (270 MHz, CD_3OD) δ 8.88 (1H, dd, J_1 5.9 Hz, J_2 1.5 Hz, H_1), 8.36 (1H, dd, J_1 5.9 Hz, J_2 1.5 Hz, H_3), 7.59 (4H, m, H_2, H_5, H_6 and H_7), 4.78 (2H, d, J 8.4 Hz, H_{10}), 4.28 (4H, m, H_{11}), 1.32 (6H, m, H_{12}). ^{13}C{^{1}H} NMR (62.9 MHz, CD_3OD) δ 154.26 (d, J_{C-P} 9.8 Hz, C_8), 150.83 (C_1), 140.11 (C_9), 139.28 (C_3), 131.38 (C_4), 128.54 (C_6), 123.55 (C_2), 122.98 (C_5), 113.04 (C_7), 65.24 (d, J_{C-P} 6.3 Hz, C_{11}), 64.15 (d, 179.6 Hz, C_{10}), 16.93 (C_{12}), 16.84 (C_{12}). ^{31}P{^{1}H} NMR (103.90 MHz, CD_3OD) δ 22.5 IR (cm^{-1}) 2356w, 1584m (C═C), 1508(C═C), 1383w, 1271w, 1195s (P═O), 1122w, 1015m (P−O), 823w, 723w, 524w, 485w.

X-ray Crystallography. The intensity data were collected on a CAD-4 diffractometer using Mo Kα radiation (λ = 0.71069 Å) and ω-2θ scans at 160 or 293 K. The unit cell parameters were determined by least-squares refinement on diffractometer angles for 25 automatically centered reflections.[21] Data were corrected for absorption by empirical methods (ψ scan)[22] and for Lorentz-polarization effects by XCAD4.[23] The structures were solved by heavy-atom methods using SHELXS-97[24] and DIRDIF-99 programs[25] and were refined anisotropically (non-hydrogen atoms) by full-matrix least-squares on F^2 using SHELXL-97.[24] The H atoms were calculated geometrically and refined with a riding model except for the hydrogens in the water molecules.

The programs ORTEP-3[26] and Platon[27] were used for diagrams, and WINGX[28] was used to prepare material for publication. Crystal data and refinement details are given below.

Crystal Data. Compound 2. $C_{10}H_{10.50}I_{0.50}NO_4$ P, M = 303.11, monoclinic, a = 16.494(5) Å, b = 5.513 Å, c = 25.672(3) Å, α= 90.00°, β = 103.55°, γ =90.00°, V = 2269.4(8) Å^3, space group $A2/n$, Z = 8, D_c =1.774 Mg/m^3, μ = 1.603 mm^{-1}, reflns measured 2039, unique reflns 1990 with R_{int} = 0.0338, T = 294(2) K, final R indices {$I > 2\sigma(I)$] R1 = 0.0269, wR2 = 0.0582, and for all data R1 = 0.0548, wR2 = 0.0662. CCDC reference no. 290229.

Compound 4. $C_{14}H_{18}Cl_2NO_4PZn$, M = 431.53, monoclinic, a = 10.259(3) Å, b = 13.606(3) Å, c = 13.111(3) Å, α = 90.00°, β = 92.53(2)°, γ =90.00°, V = 1828.3(8) Å^3, space group $P21/n$, Z = 4, D_c =1.568 Mg/m^3, μ = 1.739 mm^{-1}, reflns measured 3425, unique reflns 3204 with R_{int} = 0.0182, T = 294(2) K, final R indices {$I > 2\sigma(I)$] R1 = 0.0478, wR2 = 0.1154, and for all data R1 = 0.0841, wR2 = 0.1282. CCDC reference no. 290232.

Computational Details. In this study, the relatively large size of the metal complex investigated, along with the computational speed requirements, have naturally led us to use a density-functional-based approach. Calculations were performed using CPMD[29] with density functional theory (DFT) employed in its plane wave pseudo-potential implementation. A local density approximation (LDA) was used for the electronic exchange and correlation functional, along with Goedecker norm-conserving pseudopotentials[30,31] for each atom present in the unit cell and a plane-wave energy cutoff of 150 Ry. We used a semi-core pseudopotential for the zinc atom and thus treated all 3d electrons as valence electrons. All calculations were performed in a large orthorhombic periodic supercell of 10.0 × 16.0 × 13.0 Å^3 at the γ-point of the Brillouin zone. An unconstrained optimization of the atomic positions was then carried out for the electronic ground states of both compounds **1** and **4**. We assumed that compound **4** was present in solution as a monohydrated monomer rather than a polymer (see Figure 10). The optimizations of the ionic positions were performed using a linearly scaling BFGS algorithm [32] and were terminated when the largest atomic gradient component was below 10^{-5} H b^{-1}. Selected distances and angles are reported in Table 5 for compound **4**. To model the fluorescence process, we then used a low-spin excitation scheme, ROKS, as described by Hutter and Frank,[33] to perform an optimization of the lowest singlet (S_1) excited-state geometry; this method has been shown to provide very reliable results for the geometry of low-lying excited states. Finally, we performed a TDDFT calculation, using the adiabatic local density approximation (ALDA),[34] at the optimized excited-state geometry to estimate the energy of the fluorescence transitions along with the oscillator strength and the change in dipole moment upon de-excitation (see TDDFT contributions breakdown in Table 6).

It has been shown that LDA reproduces well the geometry of Werner zinc complexes,[35] and this functional is also know to give a fair representation of the excitation spectrum using TDDFT methods at a modest computational cost.[35] To compute the fluorescence transitions, we assume that the main contribution to the fluorescence process comes from transitions from excited-state S_1 to the electronic ground state (S_0) and that the emission takes place at the minimum geometry of the S_1 state.

All calculations were performed on a cluster of Apple X-Serve computers at Queen Mary, University of London.

Acknowledgment. We are grateful to EPSRC, Air Products Plc, and Queen Mary University of London for studentship support to S.P.M. and E.B., EPSRC Mass Spectroscopy Service, Peter Haycock, Harold Toms, and Greg Coumbarides for NMR spectra.

Note Added after ASAP Publication. References to a figure and the display of a symbol were incorrect in the version published ASAP June 17, 2006; the corrected version was published June 27, 2006.

IC052085G

(23) Harms, K.; Wocadlo, S. *XCAD4−CAD4 Data Reduction*; University of Marburg: Marburg, Germany, 1995.
(24) Sheldrick, G. M. *SHELX97 [Includes SHELXS97, SHELXL97, CIFTAB]−Programs for Crystal Structure Analysis*, Release 97-2; Institüt für Anorganische Chemie der Universität: Göttingen, Germany, 1998.
(25) Beurskens, P. T.; Beurskens, G.; Bosman, W. P.; de Gelder, R.; Garcia-Granda, S.; Gould, R. O.; Israel, R.; Smits, J. M. M. *DIRDIF-99 Program System*; Crystallography Laboratory, University of Nijmegen: Nijmegen, The Netherlands, 1999.
(26) Farrugia, L. J.; ORTEP3 for Windows, *J. Appl. Crystallogr.* **1997**, *30*, 565.
(27) Spek, A. L. *PLATON, A Multipurpose Crystallographic Tool*; Utrecht University: Utrecht, The Netherlands, 1998.
(28) Farrugia, L. J. *J. Appl. Crystallogr.* **1999**, *32*, 837.
(29) *CPMD*, Copyright IBM Corp 1990−2004, Copyright MPI für Festkörperforschung Stuttgart (1997−2001).
(30) Goedecker, S.; Teter, M.; Hutter, J. *Phys. Rev. B* **1996**, *54*, 1703.
(31) Hartwigsen, C.; Goedecker, S.; Hutter, J. *Phys. Rev. B* **1998**, *58*, 3641.
(32) Billeter, S. R.; Curioni, A.; Andreoni, W. *Comput. Mater. Sci.* **2003**, *27*, 437.
(33) Frank, I.;. Hutter, J.; Marx, D.; Parrinello, M. *J. Chem. Phys* **1998**, *108*, 4060.
(34) Zangwill, A.; Soven, P. *Phys. Rev. A* **1980**, *21*, 1561.
(35) Bray, M. R.; Deeth, R. J.; Paget, V. J.; Sheen, P. D. *Int. J. Quantum Chem.* **1996**, *61*, 85.
(36) Addison, A. W.; Rao, T. N.; Reedijk, J.; van Rijn, J.; Verschoor, G. C. *J. Chem. Soc., Dalton Trans.* **1984**, 1349.